BNL-216254-2020-JAAM

Direct observation of defect-aided structural evolution in Ni-rich layered cathode

S. Li, S. Hwang

To be published in "Angewandte Chemie International Edition"

August 2020

Center for Functional Nanomaterials

Brookhaven National Laboratory

U.S. Department of Energy

USDOE Office of Science (SC), Basic Energy Sciences (BES) (SC-22)

DISCLAIMER

Direct observation of defect-aided structural evolution in Ni-rich layered cathode

Shuang Li[+], Zhenpeng Yao[+], Jianming Zheng[+], Maosen Fu, Jiajie Cen, Sooyeon Hwang, Huile Jin, Alexander Orlov, Lin Gu, Shun Wang*, Zhongwei Chen*, Dong Su*

[*] Dr. S. Li,[+] Prof. H. Jin, Prof. S. Wang
College of Chemistry and Materials Engineering
Institute of New Materials and Industrial Technologies
Wenzhou University, Wenzhou, Zhejiang, 325035, China
E-mail: shunwang@wzu.edu.cn
Dr. S. Li,[+] Prof. Z. Chen
Department of Chemical Engineering
University of Waterloo
Waterloo, Ontario, N2L 3G1, Canada
E-mail: zhwchen@uwaterloo.ca
Dr. S. Li,[+] Dr. S. Hwang, Prof. D. Su
Center for Functional Nanomaterials
Brookhaven National Laboratory
Upton, NY 11973, USA
E-mail: dongsu@iphy.ac.cn
Dr. Z. Yao[+]
Department of Chemistry and Chemical Biology
Harvard University
12 Oxford Street, Cambridge, Massachusetts 02138, United States
Department of Chemistry and Department of Computer Science
University of Toronto
Toronto, Ontario M5S 3H6, Canada
Dr. J. Zheng[+]
Energy and Environment Directorate
Pacific Northwest National Laboratory
902 Battelle Boulevard, Richland, Washington 99352, USA.
College of Chemistry and Chemical Engineering
Xiamen University
Xiamen, Fujian 361005, China
Dr. M. Fu
Shanxi Materials Analysis and Research Center, School of Materials Science and Engineering
Northwestern Polytechnical University
Xian, 710000, China
Dr. J. Cen, Prof. A. Orlov
Department of Materials Science and Chemical Engineering
Stony Brook University
Stony Brook, NY 11794, USA
Prof. L. Gu, Prof. D. Su
National Laboratory for Condensed Matter Physics, Institute of Physics
Chinese Academy of Sciences
Beijing, 100190, China
[+] These authors contributed equally to this work.

Abstract: Ni-rich $LiNi_{1-x-y}Mn_xCo_yO_2$ (NMC) layered compounds have become the dominated cathode for lithium ion batteries. The role of crystallographic defects on their structure evolution and consequent performance degradation during electrochemical cycling is not yet fully understood. Here, we investigated the structural evolution of Ni-rich NMC cathode in a solid-state cell via *in-situ* transmission electron microscopy. We identified antiphase boundary (APB) and twin boundary (TB) separating layered phases played an important role on phase change. Upon the lithium depletion, the APB extends across the layered structure, while Li/transition metal (TM) ion mixing in the layered phases is detected to induce the rock-salt phase formation along the coherent TB. According to DFT calculations, Li/TM mixing and phase transition are aided by the low diffusion barriers of TM ions at planar defects. This work reveals the dynamical scenario of secondary phase evolution, which helps to unveil the origin of performance fading in Ni-rich NMC.

Introduction

Rechargeable lithium ion batteries (LIBs) have been widely deployed in portable electronics devices and are gradually penetrating the market of transportation systems, such as electric vehicles (EVs), due to their energy density dominance over traditional energy storage apparatuses.[1] Next generation LIBs of higher energy density are urgently needed, which is intrinsically limited by the electrode materials upon (de)accommodating lithium ions capacity, especially the cathode side.[2] To replace currently commercialized cathodes of $LiCoO_2$ and $LiNi_{1/3}Mn_{1/3}Co_{1/3}O_2$ (NMC333), nickel-rich $LiNi_{1-x-y}Mn_xCo_yO_2$ (Ni-rich NMC) layered compounds have attracted significant attentions for their sizable specific discharge capacity and superb cost effectiveness.[3] However, Ni-rich NMC cathode presently suffers rapid performance degradations upon cycles (*i.e.*, capacity fading and power loss).[4]This degradation has been attributed to the structural changes initiated from the particle surface, such as the breakdown of cathode electrolyte interphase layer, [5] surface structural reconstruction, [4c, 6] surface corrosion, [5d, 7] transition metal (TM) ion dissolution, [5c, 8] as well as the bulk structural changes, including Li^+/Ni^{2+} ion exchange, [9] phases transition[10] and intergranular/intragranular cracks.[10c, 11] Those changes significantly reduce the reversible capacity owing to the blocked Li^+ diffusion path, induced anisotropic stress, and increased charge transfer resistance. [3e, 6a, 9a, 12] Previous reports on the performance-structure correlation in Ni-rich and regular NMC cathodes are summarized in Tables S1 and S2. However, these reports did not consider the effects from the crystallographic defects. It is well known that the crystallographic defects, such as dislocations, stacking faults, antiphase boundaries, and twin boundaries, commonly exist in lithium-metal-oxide electrodes. [11a, 13] Up to now, the roles of these defects on the performance decay remains elusive.

The structural defects can only be observed with transmission electron microscopy (TEM) and the technical challenge is at building a proper *in-situ* TEM cell containing liquid electrolyte. In addition, the local chemical inhomogeneity, secondary phases, and stress generated during

delithiation can affect the structural stability and increase the mobility of defects. [13d, 14] That demands a high spatial resolution observation from the same sample region and then one can distinguish local atomic structure changes. To the best of our knowledge, how these defects affecting local structural changes during the extraction of Li^+ remains unclear, and also it is not well established how the defects and secondary phases link to the material performance degradation.

In this work, we investigated the dynamical coupling of secondary phases and structural defects in Ni-rich NMC upon delithiation using *in-situ* biasing transmission electron microscopy (TEM) on a cross-sectional solid-state cell. We identified the co-existence of three different phases in the as-synthesized particle, *i.e.*, layered, spinel, and rock-salt, as well as the phase boundaries between them. Under biasing voltage, we observed the elongation of the antiphase boundary (APB), the phase transition near the coherent twin boundary (TB), and the formation of disordered rock-salt phase induced by the Li^+ extraction inside the particle. Density function theory (DFT) calculations confirmed the thermodynamic tendency of APB formation upon delithiation. We also found that the rock-salt phase appeared at the TB was due to the kinetically more facile Li/TM exchanges at TB compared to normal crystalline order area. Therefore, these phase changes were inclined to form close to planar defects either inside particle or in surface regions, suggesting critical role of defects on the degradation of electrode. Our results provided the dynamical scenario of defects and secondary phases during delithiation, which help to unveil the origin of performance fading in Ni-rich NMC.

Results and Discussion

We built a solid-state battery inside TEM with a Nanofactory biasing TEM holder, as shown in Figure 1a, to realize the *in-situ* observation of the local structural changes during delithiation. As one of the representative Ni-rich NMCs, $LiNi_{0.76}Mn_{0.14}Co_{0.10}O_2$ (NMC76) has been used as cathode, showing secondary particle with a primary particle size of about 200nm. A layer of $Li_{0.5}La_{0.5}TiO_3$ (LLTO) solid electrolyte was deposited on the surface of the NMC76 cathode by

pulsed laser deposition (PLD) to provide the lithium ion extraction path and then NMC76 secondary particle was cut and polished by a focused ion beam (FIB). The prepared specimen is shown in a low magnification high angle annular dark-field scanning TEM (HAADF-STEM) image as Figure 1b. The processes of the deposition and FIB milling are detailed in Figure S1. The Au and Pt layers deposited on the sample during FIB preparation serve as the top electrode for biasing. A negative bias is applied between the tip and sample which generates an electric field to extract lithium ion out of sample as indicated by the green arrow. The elemental distributions of the NMC76 sample is obtained with a STEM-energy dispersive X-ray Spectroscopy (EDX) mapping shown in Figure S2, where we can easily distinguish the NMC76 particle as well as LLTO, Au, and Pt layers.

The pristine NMC76 sample has a layered structure (*R-3m*) as indicated in X-ray diffraction (XRD) pattern of Figure S3, but we found here our sample contains minor spinel and rock-salt phase which can be due to the inhomogeneous chemical composition and Li/Ni cation mixing. Layered, spinel, and rock-salt phases have similar TM-O frameworks with close lattice spacings making them coherent inside grains. The layered phase has a hexagonal structure with a space group of *R-3m* (a=2.877Å b=14.228Å),[15] where the transition metal and lithium occupy octahedral 3*b* and 3*a* sites, respectively. Whereas the spinel and rock-salt phase have the space groups of *Fd-3m* (a=8.219Å) [16] and *Fm-3m* (a=4.177Å), respectively, as shown in Figure 1c. The black rhombus in each phase model indicates the similar unit cells with slightly different lattice constants (Layered: 4.98Å×5.03Å×5.75Å, spinel: 5.03Å×5.03Å×5.81Å, Rock-salt: 5.12Å×5.12Å×5.91Å). We note that the lattice parameters can vary along with the local chemical compositions. In addition, the space groups of the layered and spinel phases are subgroups of the rock-salt phase, which means traditional phase boundaries should be observed. However, from a specific zone axis, it is easy to distinguish these three phases from the high-resolution HAADF-STEM images of NMC76 sample as shown in Figure 1d, where the bright spots indicate the projection of TM columns (Z-contrast). In addition, we found some voids

(small dark areas marked by black arrows in Figure 1b) in the pristine sample, which were also reported in NMC333.[17] We did not observe any elemental inhomogeneity around these voids with STEM- electron energy loss spectroscopy (EELS) mapping (Figure S4) but we deduce these voids formed during synthesis can be possibly correlated to the Kirkendall effect.[18] In this work, no effects from voids were found on the evolutions of either defects or phases.

It is well known that lithium diffusion in layered compounds is along ***a-b*** plane which is strongly affected by phase boundaries. The projection lattice structures of the boundaries can be considered as the overlapping of the adjunct two phases. In Figure 2, we identified five kinds of boundaries in NMC76 with high-resolution HAADF-STEM imaging. The boundaries between these phases (layered, spinel, rock-salt) show a structural coherence and therefore orientational correlations, to reduce the strain energy. Figure 2a-e are HR-HAADF-STEM images of the boundaries and the corresponding schematic showing the phase orientations. Atomic models were overlapped with the boundaries with the blue circles representing TM atom columns, and cyan circles representing TM atom columns with lower occupancies. There are two typical boundaries between one layered phase with another layered phase domain. One is APB with one translation shift vector along the *c* direction, as shown in Figure 2a. In this case, the TM layer of one side is continuously contacted to the Li layer of the other side. The boundary has several unit cell widths region with strong contrasting dots in either the TM or Li layer, which implies the boundary plane is not strictly perpendicular to the TM plane. Figure 2b shows another type of high symmetry coherent twin boundary (TB) between layered phases, which is similar to that reported in $LiCoO_2$ layered material (called as $\Sigma 2$ (-114)[110] grain boundary).[13b, 14a] The zone axes of the two adjacent areas are [010] and [0-10] with their (003) planes tilted about 109.7° from each other, as shown in the right schematic. Observed in Figure 2b, there is a wide overlap area with spinel structure feature, which is different to the clear and sharp boundary as reported in $LiCoO_2$,[14a] and may be caused by the stress and the high degree of TM/Li disorder in NMC76 sample. Besides the boundaries between layered phases, the

boundaries between different phases have presented characteristics of overlapping regions, as shown in Figure 2c-e. Figure 2c shows the boundary between the layered and spinel phases, which has a spinel-like feature with a slightly different contrast at the TM atom column as the index shown. Figure 2d shows the boundary between the rock-salt and spinel phases, the center octahedral 16*c* site which is normal vacant in spinel unit cell show some bright contrast and we called it disordered spinel phase boundary. Figure 2e shows the boundary between the rock-salt and layered phases, which has a disordered layered phase feature. We note that the disordered layered phase displayed the identical feature of the ion-mixed phase. This feature can be from either overlapping or indeed the ion-mixing. Because of the similar cubic close packed oxygen arrays of these three phases, they all have a certain orientation relationship to minimize the boundary energy, as indicated in the corresponding schematic at right of Figure 2c-e: $[010]_L//[110]_S$, $(001)_L//(1\text{-}11)_S$ and $[110]_R//[110]_S$, $(1\text{-}11)_R//(1\text{-}11)_S$ and $[110]_R//[010]_L$, $(1\text{-}10)_R//(001)_L$. The boundaries between layered compounds as planar defects have been observed previously in the bulk region of delithiated or cycled NMC cathodes, [13c, 14a, 19] while the boundaries facing with other minor phase, spinel or rock-salt phase, are normally observed on particle surface. [4b, 6a] The stability of these planar defects under the extraction of lithium of NMC76 will be studied in the following sections. The boundaries of these three phases in NMC76 were analyzed in Table 1.

We compared the structural changes of identical areas with HR-STEM under biasing. Figure 3a shows a HR-HAADF-STEM image of a representative area where APB and TB between layered phases were observed in the pristine sample. These defects are thought to be origin from the materials synthesis process. Figure 3b shows the image at the same imaging conditions from the same area after delithiation. These images were filtered using an Average Background Subtraction Filter (ABSF) method to enhance the contrast to be easily distinguished and the raw images are provided in Figure S5. Combining the images before and after delithiation in Figure 3d, the APB here could be clearly confirmed by the characteristic that the TM layer of

one side is continuously contacted to the Li layer of the other side. The structural changes after delithiation are schematically shown in Figure 3c, where the APB and TB are marked by magenta and blue, respectively. The extraction of lithium is supposed along (003) plane to the upright direction. For the sake of observation, the solid and dash line are used to represent the boundaries ignoring the width of boundary. The solid lines represent boundaries before biasing, while the dash lines represent boundaries after delithiation. Comparing Figure 3a and b, there is no sign of phase transition from O3 to O1, which is consistent with prior studies.[10c, 20] Figure 3d-f are enlarged figures of the areas marked in Figure 3a and b, respectively. The APB in Figure 3d extends from 4 nm to 7.5 nm through the movement of a partial dislocation with a Burgers vector of 1/6[211]. From the images before and after delithiation, it is observed that the APBs moved faster along the ***a-b*** plane than crossing ***a-b*** plane, which is probably because the (003) plane containing vacancies at Li^+ sites is favorable for the movement of TM cations and dislocation. Besides APB, the TB at this area shifts a little along (003) plane, as shown in Figure 3c and e. From the enlarged image of Figure 3e, we found the cation mixing near the TB increased after delithiation. In Figure 3f, cation mixing is largely enhanced along the TB at the top right area of the image, where disordered rock-salt phase appears. It is concluded from above results that with delithiation the phase transition from order to disorder is prompted, especially along the planar defects (TB).

Previous studies reported the phase evolution from layered to disordered layered or spinel, and then to rock-salt close to the surface of the layered cathode particle. [6a, 6b, 7, 13a, 21] It was believed that this TM ion migration caused surface reconstruction and blocked the lithium ion diffusion channel, leading to the large irreversible capacity.[12a] Meanwhile, the formation of rock-salt phase usually accompanied by the oxygen loss which may induce capacity reduction, rapid voltage decay and lead to structure instability and thermal runaway.[4d, 11a, 16] However, some other reports suggested that the rock-salt phase on the surface can be beneficial on the reversibility due to the pillaring effect.[3c, 7, 22] Here, we also investigate the evolution of TB

close to the surface region during delithiation. We chose the surface region near the LLTO layer as shown in Figure 4a, marked by yellow arrows. From the HR-HAADF-STEM image of pristine NMC76 in Figure 4b, the TB can be easily observed, which has a broad area with a spinel phase feature (the original images are shown in Figure S6), as discussed in Figure 2b. After delithiation, the rock-salt phase appeared at the surface and kept propagating inward, as shown in Figure 4c. The Figure 4d and e are the enlarged images of the marked area of Figure 4b and c, respectively, showing the disordering atomically. There is a weak contrast in the central sites of some spinel unit cells in Figure 4d, which implies there are some cation migrations in the TB at surface area before reaction. As schematically shown in Figure 4f, the rock-salt phase near surface also extends gradually along the TB during delithiation, which is identical to what we observed inside NMC76 particle. In our *in-situ* TEM experiments, we observed the biasing indeed extracted lithium ion from the structure and then induced the structural changes along planar defects, though we could not quantify the amount of extracted Li^+.

APB was observed to extend, glide, and enlarge during the delithiation process, as shown in Figure 3. And the enlargement along (003) plane seems to be faster than perpendicular directions. To understand this phenomenon, we built a structural model of the NMC76 phase with APB introduced through partially shifting the metal layers by 1/6[211] (Figure S7). The ratio between Ni: Mn: Co is settled as 9:2:1 with the simulated stoichiometry to be $LiNi_{3/4}Mn_{1/6}Co_{1/12}O_2$, approaching the experimentally determined composition. We evaluated the thermodynamic tendency on APB formation *via* calculating the energy difference between NMC76 configurations with and without APB in a function of Li content. As shown in Figure 5a, the energy difference between the systems with APB and without APB is a small value of 57 meV/atom as the extraction of Li is $x = 0$, which indicates the possible existence of APB in as-synthesized NMC76, as we observed in Figure 2 and 3. With the extraction of Li, the energy difference increases to 110 meV/atom at $x = 0.24$ and eventually approaches zero when 0.8

lithium ion per formula has been extracted. This could happen around an APB where the lattice distortion, electronic conductivity and local chemistry can facilitate Li diffusion[13c] and prompt a Li depletion state. The calculated energy differences imply that the APB formation could occur earlier at domains where the Li depletion is more likely to occur at particle surfaces, grain boundaries, and dislocations as observed in this study.[23] The extension of APB can be attributed to gradual development of Li depletion region originated from surfaces/defects during delithiation of the particle.

Phase transformations basically proceed with the migrations of atoms inside the crystal structure, such as that the phase transition from layered structure to rock-salt is initiated with the TM diffusion to the lithium layer. Therefore, the trend of phase transition can be evaluated through computing the related energetic barriers of all ion migrations. To investigate the impact of TB on the layered → rock-salt phase transformation in NMC76, we evaluated the kinetics of a series of reaction steps around TB in the NMC76 cathode. Meanwhile, we calculated the energetic barriers of TM ion diffusion in pristine NMC76 structure as the reference. Ni, which is the mobile TM ion in our system, was picked in this study to represent the TM atoms.[6c] Structure models were built with TB along (104) interface (Figure S9) based on the experimental observations in Figure 2c. In pristine NMC76, TM(Ni) diffusion has been proven to be rather difficult with large barriers both within the TM layer (2.11 eV) and from the TM layer to the Li layer (1.20 eV), as shown in Figure 5b, indicating the difficulty of any TM migration related phase transition in pristine NMC76. For the NMC76 with a TB, we first calculated the barrier of the vacancy assisted Li diffusion along the TB (i), as shown in Figure 5c. A small value of 0.41 eV was obtained, implying the relatively fast Li transport along the boundary during the Li extraction. Moreover, the removal of Li in the boundary creates vacancies to facilitate the following TM (Ni) migration (ii) from the TM layer to the Li layer. An anisotropic barrier (Figure 5d) is observed with a modest forward barrier of 0.68 eV implies

the notable potential for the initiation of layered → rock-salt phase transition. However, a larger backward barrier of 0.94 eV indicates the difficulty for Ni to migrate back to its original position shedding light on the irreversible layered → rock-salt phase transition. Then we calculated the TM (Ni) diffusion barrier towards the boundary (iii), as shown in Figure 5e with a rather small barrier of 0.26 eV obtained. Afterward, many of the TM (Ni) ions will continue to make a further migration step to the Li layer as in the (ii) step. Therefore, the facile TM (Ni) migration towards TB can be seen as a sign that more and more TM ions will diffuse to the Li layer and participate in the phase transition, which will eventually lead to the growth of the rock-salt phase. As a result, the presence of TB facilitates both the initiation and development of the layered → rock-salt phase transition, confirming the experimental observations that the rock-salt phase grows around the TB in the NMC76 particle. The experimental and consistent simulation results concurrently imply that the Li ion diffusion is strongly affected by these two defects during delithiation. In particular, the TB would facilitate the TM migration and then phase transition which could have a detrimental effect on the battery performance.

Conclusion

In summary, the structural evolution of Ni-rich NMC76 cathode during delithiation was investigated by *in-situ* TEM. Distinguished from previous works which generally focused on the phase transitions at particle surfaces, we here confirmed for the first time the formation of secondary phase inside the particle aided by crystallographic defects. We classified the boundaries between three phases (layered, spinel, rock-salt), namely APB, TB, spinel-like, disordered spinel and disordered layered, and identified them with high-resolution STEM imaging. Under *in-situ* biasing, we found the extension of APB induced by delithiation. The formation energy of APB can be largely decreased upon deep lithium ion deintercalation as suggested by DFT calculations. On the other hand, the increasing Li/TM mixing or appearance of rock-salt phase were observed around TB after delithiation, in both surface and bulk region.

Our calculations indicate TB can provide a feasible diffusion pathway for Li and TM migration with smaller energetic barriers, resulting in disordering and rock-salt phase formation. Structurally, the propagation of APB with blocked Li diffusion path may result in increased resistance for Li ion extraction and intercalation, meanwhile, the phase transition towards rock-salt phase will aggravate the electrode degradation during battery cycling. Our studies indicated that the degradation mechanisms of the Ni-rich NMC material are beyond surface determined, the inhomogeneous lithium extraction and TM migration caused by defects inside the bulk also show a significant impact. Our study can assist the development of the effective approach in suppressing secondary phase formation and design Ni-rich NMC electrodes with improved cyclability for high energy density LIBs.

Acknowledgements

This work was supported by the University of Waterloo and Wenzhou University, the National Natural Science Foundation of China (U1909213, 51772219 and 51872209). This research used resources of the Center for Functional Nanomaterials, which is a U.S. DOE office of Science Facility, at Brookhaven National Laboratory under contract No. DE-SC0012704. Computations were performed on the niagara supercomputer at the SciNet HPC Consortium. SciNet is funded by: the Canada Foundation for Innovation; the Government of Ontario; Ontario Research Fund - Research Excellence; and the University of Toronto.

Conflict of Interest

The authors declare no conflict of interest.

Keywords

cathode materials, lithium ion batteries, in-situ transmission electron microscopy, defect, phase transition

References

[1] a) J. M. Tarascon, M. Armand, *Nature* **2001**, 414, 359-367; b) V. Etacheri, R. Marom, R. Elazari, G. Salitra, D. Aurbach, *Energy Environ. Sci.* **2011**, 4, 3243; c) H. Li, *Joule* **2019**, 3, 911-914.

[2] a) J. B. Goodenough, Y. Kim, *Chem. Mater.* **2010**, 22, 587-603; b)J. W. Choi, D. Aurbach, *Nat. Rev. Mater.* **2016**, 1, 16013.

[3] a) K. Kang, Y. S. Meng, J. Bréger, C. P. Grey, G. Ceder, *Science* **2006**, 311, 977-980; b) H.-J. Noh, S. Youn, C. S. Yoon, Y.-K. Sun, *J. Power Sources* **2013**, 233, 121-130; c) C. S. Yoon, M. H. Choi, B.-B. Lim, E.-J. Lee, Y.-K. Sun, *J. Electrochem. Soc.* **2015**, 162, A2483-A2489; d) J. Li, H. Liu, J. Xia, A. R. Cameron, M. Nie, G. A. Botton, J. R. Dahn, *J. Electrochem. Soc.* **2017**, 164, A655; e) W. Liu, P. Oh, X. Liu, M. J. Lee, W. Cho, S. Chae, Y. Kim, J. Cho, *Angew. Chem. Int. Ed. Engl.* **2015**, 54, 4440-4457.

[4] a) A. Manthiram, J. C. Knight, S.-T. Myung, S.-M. Oh, Y.-K. Sun, *Adv. Energy Mater.* **2016**, 6, 1501010; b) Q. Lin, W. Guan, J. Meng, W. Huang, X. Wei, Y. Zeng, J. Li, Z. Zhang, *Nano Energy* **2018**, 54, 313-321; c) Q. Wang, C. H. Shen, S. Y. Shen, Y. F. Xu, C. G. Shi, L. Huang, J. T. Li, S. G. Sun, *ACS Appl. Mater. Interfaces* **2017**, 9, 24731-24742; d) X. Cheng, J. Zheng, J. Lu, Y. Li, P. Yan, Y. Zhang, *Nano Energy* **2019**, 62, 30-37; e) H. Kim, M. G. Kim, H. Y. Jeong, H. Nam, J. Cho, *Nano Lett.* **2015**, 15, 2111-2119; f) T. Li, X.-Z. Yuan, L. Zhang, D. Song, K. Shi, C. Bock, *Electro. ener. rev.* **2019**.

[5] a) P. Yang, J. Zheng, S. Kuppan, Q. Li, D. Lv, J. Xiao, G. Chen, J.-G. Zhang, C.-M. Wang, *Chem. Mater.* **2015**, 27, 7447-7451; b) K. Xu, *Chem. Rev.* **2014**, 114, 11503-11618; c) D. Li, H. Li, D. L. Danilov, L. Gao, X. Chen, Z. Zhang, J. Zhou, R.-A. Eichel, Y. Yang, P. H. L. Notten, *J. Power Sources* **2019**, 416, 163-174; d) W. Zhao, J. Zheng, L. Zou, H. Jia, B. Liu, H. Wang, M. H. Engelhard, C. Wang, W. Xu, Y. Yang, J.-G. Zhang, *Adv. Energy Mater.* **2018**, 8, 1800297.

[6] a) S.-K. Jung, H. Gwon, J. Hong, K.-Y. Park, D.-H. Seo, H. Kim, J. Hyun, W. Yang, K. Kang, *Adv. Energy Mater.* **2014**, 4, 1300787; b) F. Lin, I. M. Markus, D. Nordlund, T. C. Weng, M. D. Asta, H. L. Xin, M. M. Doeff, *Nat. Commun.* **2014**, 5, 3529; c) P. Yan, J. Zheng, J. G. Zhang, C. Wang, *Nano Lett.* **2017**, 17, 3946-3951; d) S. Hwang, S. M. Kim, S.-M. Bak, K. Y. Chung, W. Chang, *Chem. Mater.* **2015**, 27, 6044-6052.

[7] Y. Cho, P. Oh, J. Cho, *Nano Lett.* **2013**, 13, 1145-1152.

[8] M. Börner, F. Horsthemke, F. Kollmer, S. Haseloff, A. Friesen, P. Niehoff, S. Nowak, M. Winter, F. M. Schappacher, *J. Power Sources* **2016**, 335, 45-55.

[9] a) H. Yu, Y. Qian, M. Otani, D. Tang, S. Guo, Y. Zhu, H. Zhou, *Energy Environ. Sci.* **2014**, 7, 1068-1078; b) J. Zheng, Y. Ye, T. Liu, Y. Xiao, C. Wang, F. Wang, F. Pan, *Acc. Chem. Res.* **2019**, 52, 2201-2209.

[10] a) J. Shu, R. Ma, L. Shao, M. Shui, K. Wu, M. Lao, D. Wang, N. Long, Y. Ren, *J. Power Sources* **2014**, 245, 7-18; b) S. S. Zhang, *J. Energy Chem.* **2020**, 41, 135-141; c) H.-H. Ryu, K.-J. Park, C. S. Yoon, Y.-K. Sun, *Chem. Mater.* **2018**, 30, 1155-1163.

[11] a) P. Yan, J. Zheng, T. Chen, L. Luo, Y. Jiang, K. Wang, M. Sui, J. G. Zhang, S. Zhang, C. Wang, *Nat. Commun.* **2018**, 9, 2437; b) H. Zhang, F. Omenya, P. Yan, L. Luo, M. S. Whittingham, C. Wang, G. Zhou, *ACS Energy Lett.* **2017**, 2, 2607-2615.

[12] a) M. N. Obrovac, O. Mao, J. R. Dahn, *Solid State Ion.* **1998**, 112, 9-19; b) K. Kang, G. Ceder, *Phys. Rev. B* **2006**, 74, 094105; c) J. Lee, A. Urban, X. Li, D. Su, G. Hautier, G. Ceder, *Science* **2014**, 343, 519-522.

[13] a) M. Gu, I. Belharouak, J. Zheng, H. Wu, J. Xiao, A. Genc, K. Amine, S. Thevuthasan, D. R. Baer, J.-G. Zhang, N. D. Browning, J. Liu, C. Wang, *ACS Nano* **2013**, 7, 760-767; b) H. Moriwake, A. Kuwabara, C. A. Fisher, R. Huang, T. Hitosugi, Y. H. Ikuhara, H. Oki, Y. Ikuhara, *Adv. Mater.* **2013**, 25, 618-622; c) P. V. Ong, Z. Yang, P. V. Sushko, Y. Du, *J Phys Chem Lett* **2018**, 9, 5515-5520; d) Q. Li, Z. Yao, E. Lee, Y. Xu, M. M. Thackeray, C. Wolverton, V. P. Dravid, J. Wu, *Nat. Commun.* **2019**, 10, 1692.

[14] a) Y. Gong, J. Zhang, L. Jiang, J. A. Shi, Q. Zhang, Z. Yang, D. Zou, J. Wang, X. Yu, R. Xiao, Y. S. Hu, L. Gu, H. Li, L. Chen, *J. Am. Chem. Soc.* **2017**, 139, 4274-4277; b) Y. Gong, Y. Chen, Q. Zhang, F. Meng, J. A. Shi, X. Liu, X. Liu, J. Zhang, H. Wang, J. Wang, Q. Yu, Z. Zhang, Q. Xu, R. Xiao, Y. S. Hu, L. Gu, H. Li, X. Huang, L. Chen, *Nat. Commun.* **2018**, 9, 3341.

[15] J. Zheng, P. Yan, L. Estevez, C. Wang, J.-G. Zhang, *Nano Energy* **2018**, 49, 538-548.

[16] S. M. Bak, E. Hu, Y. Zhou, X. Yu, S. D. Senanayake, S. J. Cho, K. B. Kim, K. Y. Chung, X. Q. Yang, K. W. Nam, *ACS Appl. Mater. Interfaces* **2014**, 6, 22594-22601.

[17] P. Yan, J. Zheng, M. Gu, J. Xiao, J. G. Zhang, C. M. Wang, *Nat. Commun.* **2017**, 8, 14101.

[18] V. Pimenta, M. Sathiya, D. Batuk, A. M. Abakumov, D. Giaume, S. Cassaignon, D. Larcher, J.-M. Tarascon, *Chem. Mater.* **2017**, 29, 9923-9936.

[19] Z. Yang, P. V. Ong, Y. He, L. Wang, M. E. Bowden, W. Xu, T. C. Droubay, C. Wang, P. V. Sushko, Y. Du, *Small* **2018**, e1803108.

[20] a) K. Märker, P. J. Reeves, C. Xu, K. J. Griffith, C. P. Grey, *Chem. Mater.* **2019**, 31, 2545-2554; b) J. Li, L. E. Downie, L. Ma, W. Qiu, J. R. Dahn, *J. Electrochem. Soc.* **2015**, 162, A1401-A1408.

[21] A. Boulineau, L. Simonin, J. F. Colin, C. Bourbon, S. Patoux, *Nano Lett.* **2013**, 13, 3857-3863.

[22] a) Y. Makimura, S. Zheng, Y. Ikuhara, Y. Ukyo, *J. Electrochem. Soc.* **2012**, 159, A1070-A1073; b) J. Xiao, N. A. Chernova, M. S. Whittingham, *Chem. Mater.* **2008**, 20, 7454-7464.

[23] R. Malik, D. Burch, M. Bazant, G. Ceder, *Nano Lett.* **2010**, 10, 4123-4127.

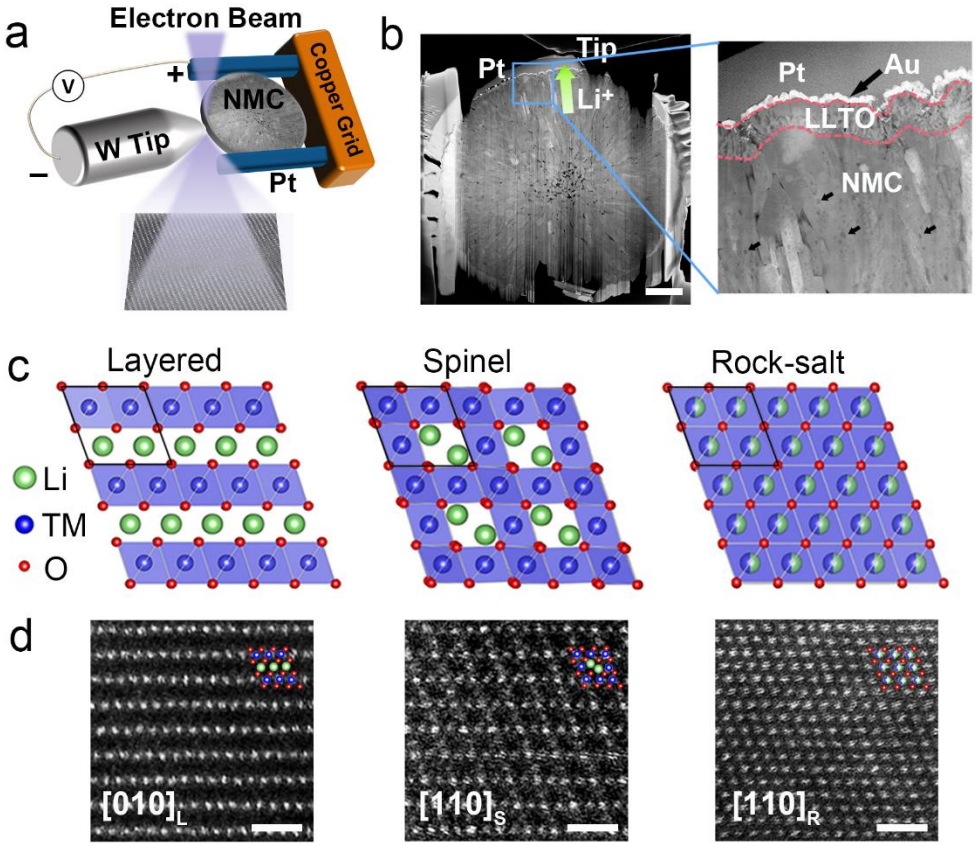

Figure 1. *In-situ* TEM setup and the atomic structure of the phases in NMC76. a) Schematic illustration of the *in-situ* TEM experimental setup. b) Corresponding low magnification HAADF-STEM images showing the components of top electrode, LLTO solid electrolyte, and NMC76. The green arrow indicates the approximate direction of lithium extraction. The atomic structural models (c) and corresponding high resolution HAADF-STEM images (d) of the layer, spinel and rock-salt phases, respectively. The black rhomboids indicate the similar unit cells with cubic close packed oxygen arrays. The subscript: L: layered, S: spinel, R: rock-salt.

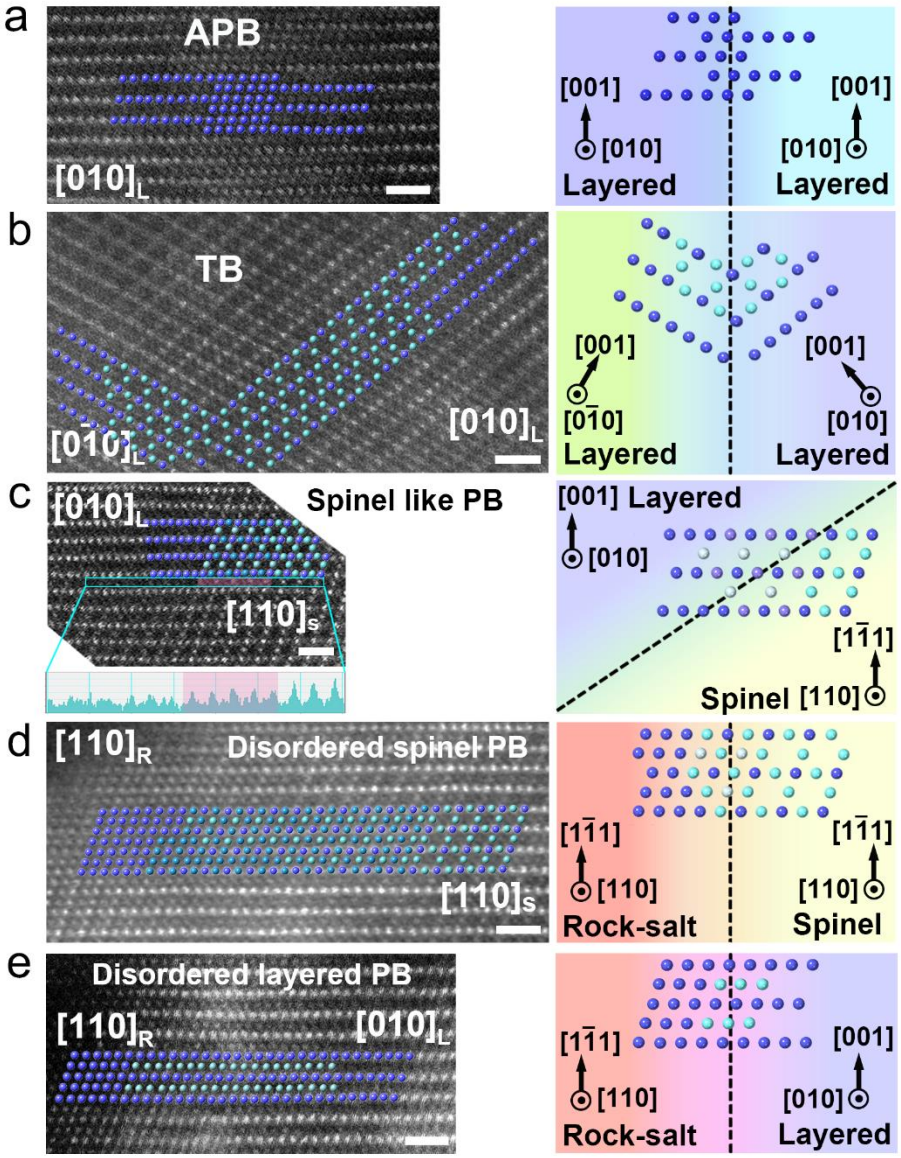

Figure 2. Atomic structure of the phase boundaries observed in NMC76. HR-HAADF-STEM images and corresponding schematic showing the phase orientations of (a) APB between layered phases, (b) TB between layered phases, (c) spinel like phase boundary between layered phase and spinel phase, (d) disordered spinel phase boundary between rock-salt phase and spinel phase near the surface region, (e) disordered layered phase boundary between rock-salt phase and layered phase near the surface region. The blue spots represent TM atomic columns, cyan spots represent TM atomic columns with lower occupancies.

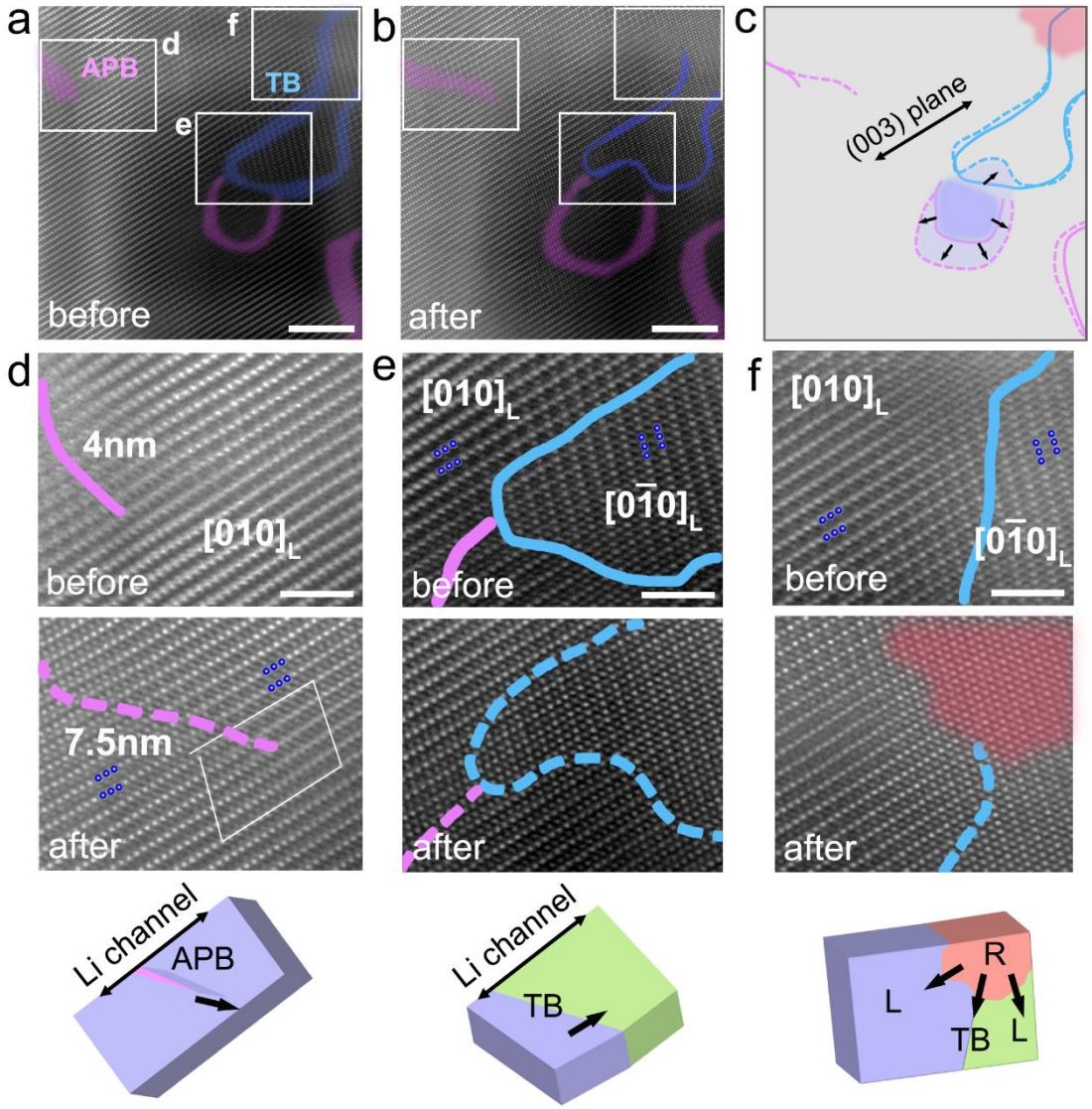

Figure 3. Interior structural changes before and after delithiation. a, b) HR-HAADF-STEM images of the same region before and after delithiation. The magenta and blue areas marked APB and TB, respectively. c) The schematic illustration showing the phases extension and defects migration extract by comparing (a) and (b). The solid lines represent boundaries before reaction, while the dash lines represent boundaries after reaction. The red and purple areas display the layered and rock-salt phases. d-f) The enlarged images of white rectangles in (a) and (b), and corresponding schematics. The black arrows indicate the phase extension directions and also the lithium ion diffusion channels.

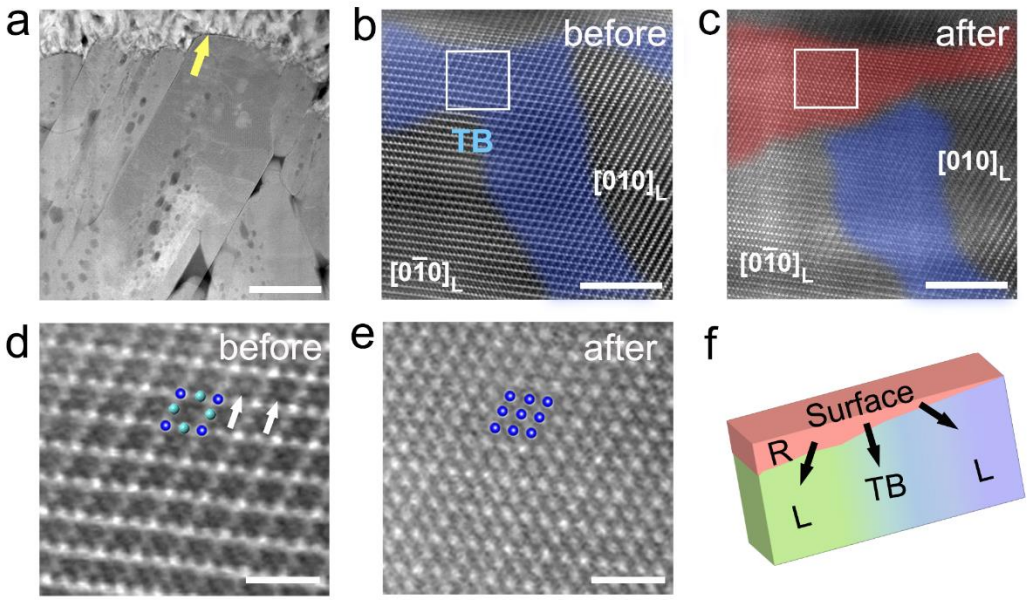

Figure 4. Structural evolution close to the surface region. a) The low magnification HAADF-STEM image of the observed primary particle. The filtered atomic scale HAADF-STEM images before (b) and after (c) delithiation of the surface region marked by yellow arrow. The blue and red areas marked TB and rock-salt phase, respectively. d, e) The enlarge images of white rectangles in (b) and (c) showing the spinel and rock-salt phases features. The white arrows indicate the weak light contrasts in the central sites of unit cells. f) The schematic illustration showing the rock-salt phase generates at the surface after delithiation.

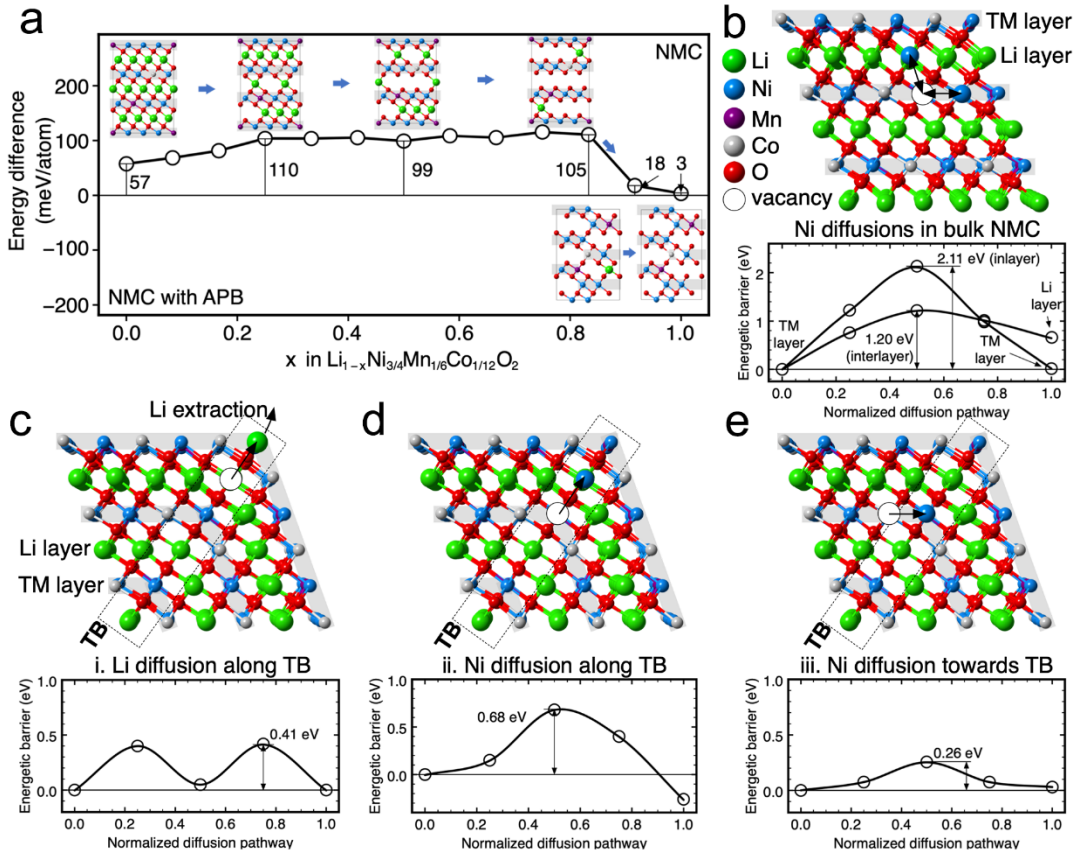

Figure 5. Calculations on the thermodynamic tendency of anti-phase boundary formation and the energetic impact of the twin boundary on the kinetics of TM ions migration in the Ni-rich NMC structure. a) The energy difference between the systems with APB and without APB. The inserts are the thermodynamically stable structure at different delithiation state. b) TM(Ni) diffusion pathways in the pristine Ni-rich NMC: in the TM layer and from TM layer to Li layer. c-e) The kinetics of a series of reaction steps required by the layered → rock-salt phase transformation. The Li diffusion along the TB (c), which creates vacancies to facilitate the following step TM(Ni) migration from the TM layer to the Li layer (d) to initiate the phase transition. Then, the TM(Ni) diffusion towards the boundary (e) to assist the development of the phase transition.

Table 1. Boundary types between different phases.

	Layered	**Spinel**	**Rock salt**
Layered	APB/ Twin boundary	Spinel like	Disordered layered
Spinel	Spinel like	Spinel	Disordered spinel
Rock salt	Disordered layered	Disordered spinel	Rock salt